Naval Surface Warfare Center
Carderock Division
9500 MacArthur Boulevard, West Bethesda, MD 20817-5700

NSWCCD-50-TR–2002/009 January 2002

Hydromechanics Directorate Report

Model and Full Scale Predictions of a Carrier Flow Field

by

Joseph Gorski, Henry Haussling and Roderick Coleman

REPORT DOCUMENTATION PAGE

Form Approved
OMB No. 0704-0188

1. AGENCY USE ONLY *(Leave blank)*	2. REPORT DATE	3. REPORT TYPE AND DATES COVERED
	January 2002	Final 9/00 - 5/01

4. TITLE AND SUBTITLE
Model and Full Scale Predictions of a Carrier Flow Field

5. FUNDING NUMBERS
WU - 5400 - 112

6. AUTHOR(S)
Joseph Gorski, Henry Hausling and Roderick Coleman

7. PERFORMING ORGANIZATION NAME(S) AND ADDRESS(ES)
Naval Surface Warfare Center
Carderock Division
9500 MacArthur Boulevard
West Bethesda, MD 20817-5700

8. PERFORMING ORGANIZATION REPORT NUMBER
NSWCCD-50-TR–2002/009

9. SPONSORING/MONITORING AGENCY NAME(S) AND ADDRESS(ES)

10. SPONSORING/MONITORING AGENCY REPORT NUMBER

11. SUPPLEMENTARY NOTES

12a. DISTRIBUTION CODE

12b. DISTRIBUTION/AVAILABILITY STATEMENT
Approved for public release; distribution is unlimited

13. ABSTRACT ***(Maximum 200 words)***

Viscous flow calculations using the Reynolds Averaged Navier-Stokes (RANS) equations are performed for a carrier configuration at both model and full scale Reynolds numbers. These calculations are for a bare hull with skeg, bilge keels and outboard propeller shaft. The calculations indicate there are extensive differences between the model and full scale wakes entering the propeller disks. Without the propeller shaft the dominant effect is the bilge vortex particularly at model scale. At full scale the flow entering the propellers is very nearly inviscid without the shafts present. The shaft wake is shown to have a significant impact on the flow entering the propeller and shaft rotation further impacts this inflow.

14. SUBJECT TERMS			15. NUMBER OF PAGES
propeller shaft	Viscous Wakes	Bilge Vortices	27
			16. PRICE CODE

17. SECURITY CLASSIFICATION OF REPORT	18. SECURITY CLASSIFICATION OF THIS PAGE	19. SECURITY CLASSIFICATION OF ABSTRACT	20. LIMITATION OF ABSTRACT
UNCLASSIFIED	UNCLASSIFIED	UNCLASSIFIED	SAR

NSN 7540-01-280-5500

Standard Form 298 (Rev. 2-89)
Prescribed by ANSI Std. Z39-18
298-102

CONTENTS

Page

ABSTRACT 1
ADMINISTRATIVE INFORMATION 1
INTRODUCTION 1
FLOW SOLVER 3
GRID GENERATION 4
FLOW SOLUTIONS 7
Bare Hull Model Scale Calculations 9
Bare Hull Full Scale Calculations 15
Outboard Shaft Effects 17
Propeller Modeling 21
Shaft Rotation Effects 23
CONCLUSIONS 25
ACKNOWLEDGEMENTS 25
REFERENCES 27

FIGURES

Page

1 Carrier hull form. 2
2 Computational grid on the water surface. 4
3 Surface grid without the shaft, view from underneath the hull 5
4 Surface grid with the outboard shaft, view from underneath the hull. 5
5 Grid blocking scheme for the hull with shaft 6
6 Cross section of grid with and without outboard shaft. 7
7 Computed wave heights. 8
8 Computed hull free surface height as compared with experimental data. 8
9 Surface streamlines and axial velocity contours for the model scale calculation. 9
10 Flow field in the bow region. 10
11 Flow field in the midships region. 10

12 Flow field in the stern region at model scale. 11
13 Axial velocity contours and secondary flow streamlines at X/L = 0.5. 12
14 Axial velocity contours and secondary flow streamlines at X/L = 0.55. 12
15 Axial velocity contours at the inboard propeller plane computed without bilge keels compared with measured[14] contours in the propeller disk. 13
16 Axial velocity contours at the inboard propeller plane computed with bilge keels compared with measured[14] contours in the propeller disk. 13
17 Axial velocity contours at the outboard propeller plane computed with bilge keels. 14
18 Computed axial velocity contours at the outboard propeller plane compared with measured[14] contours in the propeller disk. 14
19 Axial velocity contours and surface streamlines for the full-scale calculation. 15
20 Axial velocity contours at the inboard propeller plane. 16
21 Axial velocity contours at the outboard propeller plane. 16
22 Computed axial velocity contours with the outboard shaft at model scale. 17
23 Comparison of axial velocity at outboard propeller plane with/without shaft. 18
24 Secondary velocity vectors at the outboard propeller plane. 18
25 Computed and measured[14] axial velocity at the outboard propeller plane. 19
26 Computed axial velocity contours at the inboard propeller plane. 20
27 Comparison of axial velocity at the inboard propeller plane. 20
28 Model scale axial velocity with the outboard propeller modeled. 21
29 Secondary velocity vectors with the outboard propeller modeled. 22
30 Full scale axial velocity contours with the outboard propeller modeled. 22
31 Axial velocity contours with the shaft rotating. 23
32 Model scale calculation with shaft rotation. 24
33 Full-scale calculation with shaft rotation. 24

ABSTRACT

Viscous flow calculations using the Reynolds Averaged Navier-Stokes (RANS) equations are performed for a carrier configuration at both model and full scale Reynolds numbers. These calculations are for a bare hull with skeg, bilge keels and outboard propeller shaft. The calculations indicate there are extensive differences between the model and full scale wakes entering the propeller disks. Without the propeller shaft the dominant effect is the bilge vortex, particularly at model scale. At full scale the flow entering the propellers is very nearly inviscid without the shafts present. The shaft wake is shown to have a significant impact on the flow entering the propeller and shaft rotation further impacts this inflow.

ADMINISTRATIVE INFORMATION

The work described in this report was performed by the Propulsion and Fluid Systems Department (Code 5400) within the Hydrodynamics Directorate at the Naval Surface Warfare Center, Carderock Division (NSWCCD). The NSWCCD Work Unit was 00-1-5400-112.

INTRODUCTION

To better understand the flow into the propeller disk of a carrier hull form a Reynolds-Averaged Navier-Stokes (RANS) code is used to compute the flow fields about both model- and full-scale carrier hulls. The flow into the propellers is significantly influenced by the upstream hull form. This includes the boundary layer generated on the hull as well as any vortical flow that may form such as from the bow/sonar dome or bilges. Additionally, wakes are formed from upstream bilge keels, shafts, and supporting struts. RANS codes provide a means of predicting such flow fields (Gorski[1]).

The computer advances in the last decade have been a significant catalyst for improving our ability to predict ships flows. The increased computer power has led to RANS calculations on large grids being more routine. It has also led to an increased experience base as it became possible to do more calculations and trade off studies. In 1996 ITTC[2] concluded that RANS codes had matured enough to be integrated into the design process for addressing issues associated with resistance and propulsion. Such computations also provide both an overall picture and an increased understanding of the flow field in the immediate vicinity of the ship. A number of RANS codes have been able to demonstrate good results for a variety of complicated ship flow fields (Gorski[3]). To better estimate the quality of a solution there have been efforts to develop uncertainty estimates and validation procedures for computations (e.g. Refs. 4,5). This is an area of significant importance as the computational community tries to provide metrics for the quality of a computation and more work needs to be done in this area. To this end though, it is becoming largely recognized that one cannot declare a particular code validated, even with good predictions for a particular flow, because a particular solution depends on many factors including: geometry definition, grid quality, turbulence modeling and user experience among other variables. However, when applying well developed RANS codes properly, experienced users can obtain very meaningful information on complicated hull flows, including hull

modification and scale effects, without a formal validation procedure, such as the demonstrated here for a carrier vehicle.

Fig. 1 shows major features of the carrier. These include a bulbous bow, a transom stern, bilge keels, a docking skeg, propeller shafts and struts (not shown). Only the flow below the waterline, depicted in the figure, is computed. The current effort uses structured grids which makes it very difficult to include all of this complexity in the calculations. Consequently, the calculations are first performed with a bare hull configuration, which does not contain the shafts and struts for the propellers. The final computations contain the outer shaft, but do not contain the inboard shaft/strut arrangement or the outboard struts supporting the shaft, due to time constraints. Although only the outer shaft is included in the later calculations it is shown to have a significant impact on the flow into the outboard propeller. In the future including all the complexity of interest should become more feasible as the use of unstructured RANS codes becomes more routine. The calculations of interest are carried out on the full-scale hull to produce understanding of the real flow. Calculations are carried out on the model scale hull for verification and validation of the computational approach. Besides model and full scale predictions, calculations are also performed with the propeller modeled as an actuator disk and with the shaft rotating to highlight individual effects.

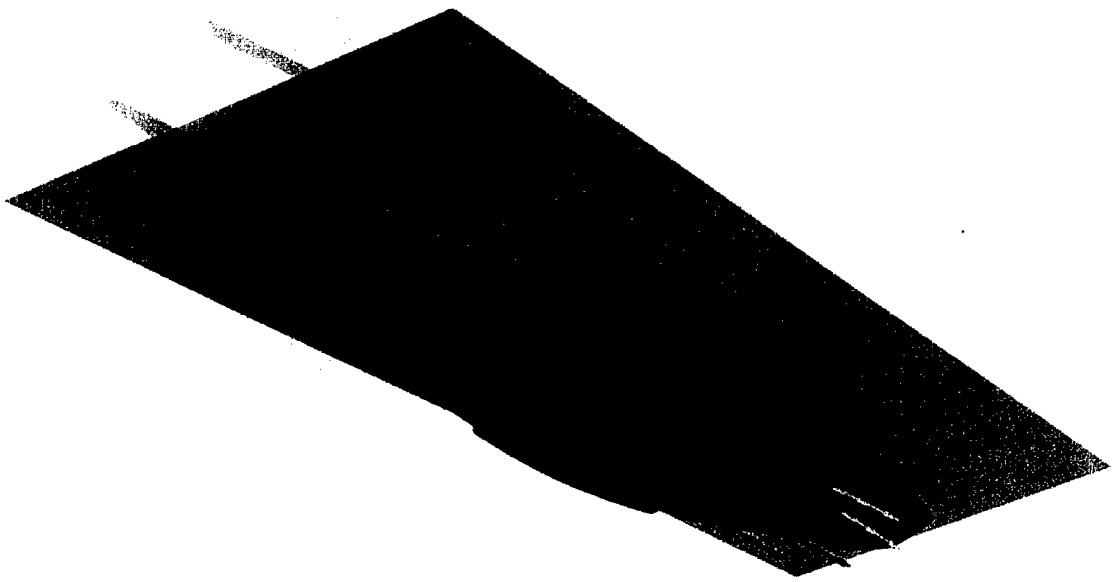

Fig. 1 Carrier hull form.

FLOW SOLVER

To compute the viscous flow field the incompressible Reynolds Averaged Navier-Stokes equations are solved using the Mississippi State University code UNCLE[6,7]. The UNCLE code is one of two RANS codes used for the ONR Surface Combatant Accelerated Hydro S&T Initiative to provide documented computational solutions for innovative propulsor/hull concepts of interest for DD-21 and beyond. The equations are solved using the pseudo-compressibility approach of Chorin[8] where an artificial time term is added to the continuity equation and all of the equations are marched in this artificial time to convergence. Only steady state computations are performed for this effort. For the present calculations a third-order upwind biased discretization, based on the MUSCL approach of Van Leer et al.[9], is used for the convective terms. The equations are solved implicitly using a discretized Newton-relaxation method[10] with multigrid techniques implemented for faster convergence[11]. The turbulence model used for the present calculations is a k-ε model. An important factor in being able to compute and evaluate the hull modifications and operating conditions of interest is the implementation of a parallel version of the UNCLE code[12]. The code uses MPI for message passing due to its portability. To run in parallel the computational grid is decomposed into various blocks, which are sent to different processors. Load balancing is obtained by making the blocks as equally sized as possible. For the present calculations 44, 84, and 166 processors are used for various grids, which included a coarse grid for bare hull, a fine grid for bare hull with bilge keels, and a fine grid containing the outboard shaft, respectively. More details of the solver can be found in the various references provided.

RANS calculations for predicting full-scale ship flows are becoming more routine. However, there are issues involved in the full scale calculations in addition to the need for more grid points for boundary layer resolution. Surface roughness is often ignored, (Patel[13]), as in the current full scale simulations, but can be important for the actual boat. Models tested are often hydrodynamically smooth allowing surface roughness to be ignored. Real ships are considerably rougher as built and only worsen with time at sea. Hence, the full scale computations probably predict thinner boundary layers than actually exist and care must be taken when interpreting the results.

Computations are carried out with both "double-model" and free-surface conditions applied at the water surface. The "double-model" condition simulates the flow about the "double body" formed by reflecting the hull about the undisturbed water level. The undisturbed water level is treated as a symmetry plane and the vertical velocity is set to zero. The "double-model" condition is a good approximation to a free-surface condition if the speed of the hull is very low or if the flow region of interest is sufficiently far from the water surface. In order to assess the impact of the water surface, computations are also carried out with free-surface boundary conditions. Inviscid free-surface conditions are applied since free-surface viscous layers are not of interest here. The shape of the water surface is computed subject to the conditions that the flow is tangential to this surface and that the pressure is atmospheric. The linearized free-surface option of the code is used where these conditions are applied at the undisturbed water level rather than at the actual computed free-surface level. This option avoids the complication of having to move the grid to conform to the free-surface shape as it is computed. Linearization is a good approximation if the wave slopes are small enough or if the flow region of interest is sufficiently far from the water surface. Comparison of results obtained with the "double-model" condition with those obtained with the free-surface conditions and with measured data shows, that for the

purposes of this study, use of the double-model condition can be quite sufficient. Also, use of linear free-surface conditions is sufficient to capture the small free-surface effects.

GRID GENERATION

An important element of the current effort is obtaining a good computational grid. For the given predictions the computations are limited to one-half the flow region by taking advantage of the port/starboard symmetry. Various structured grids are employed ranging from one of about 2.5 million points, used for preliminary computations of the hull with neither bilge keels nor propeller shafts, one of 5.9 million points, which includes bilge keels, and one of about 7.2 million points including the outboard shaft. All grids are of H-O topology with grid lines wrapping around the hull from the center plane to the undisturbed water level in transverse cross sections. For the finer grids this consists of 129 points. Radial lines, which have 129 points for the finer grids, extend from the hull outward to a far field boundary about one body length from the hull centerline. In horizontal sections grid lines wrap around the bow but continue past the transom to the downstream boundary about two body lengths from the stern. A transom grid section fills in the trough extending from the transom to the downstream boundary. A top view of the grid at the waterline is shown in Fig. 2. For the 5.9 million point grid there are 225 points along the length of the hull. The surface grid on the hull in the stern region is show in Fig. 3 where the clustering toward the skeg and bilge keel can be seen. For the grid with the outboard shaft 305 additional points are inserted longitudinally in the shaft region for better definition (Fig. 4).

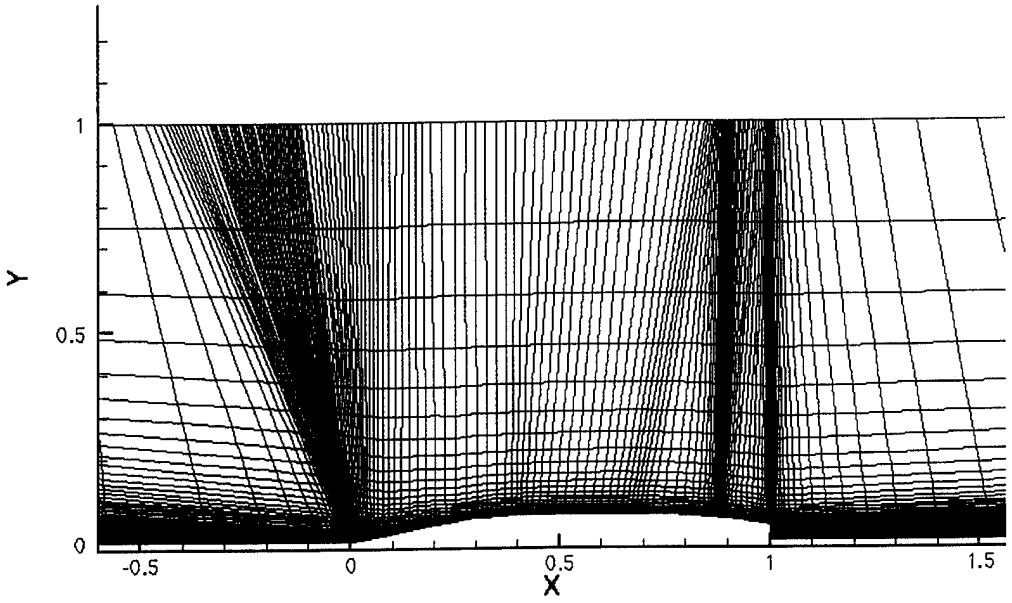

Fig. 2 Computational grid on the water surface.

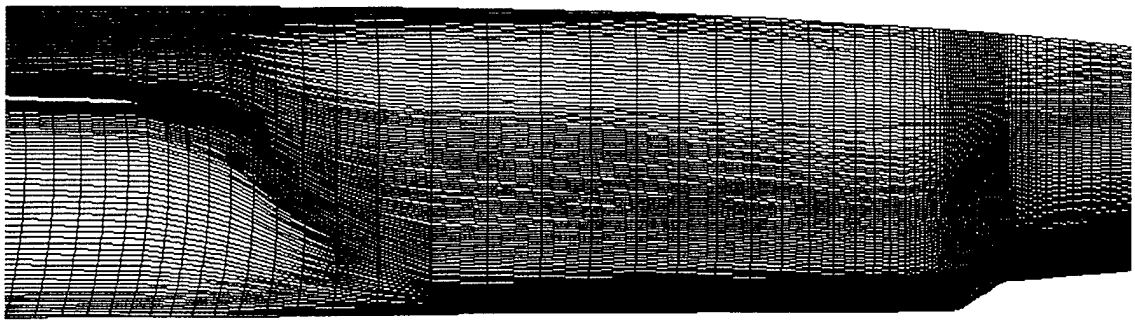

Fig. 3 Surface grid without the shaft, view from underneath the hull.

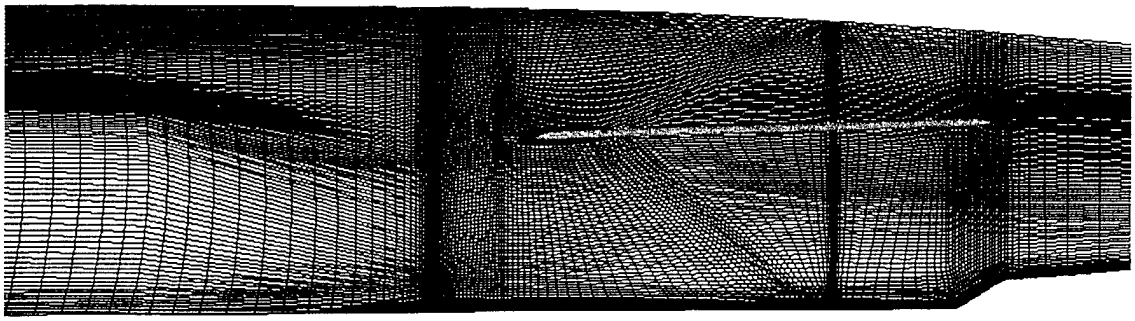

Fig. 4 Surface grid with the outboard shaft, view from underneath the hull.

The nearest points to the hull are about 10^{-6} body lengths from the wall for the model scale grid. This tight clustering is needed to ensure that the minimum spacing normal to the body surface is less than a y^+ value of 5, with a value around 1 being preferred for good behavior of the turbulence model. As one goes to higher Reynolds numbers, it is required that the relative distance of the first point off of the wall become smaller. For the current full scale computations these nearest centroid points are about 10^{-8} body lengths from the wall to yield a y^+ value less than 5. Although generating the bare hull grid is rather straightforward such tight spacing at the wall for the full-scale computations can pose significant problems, particularly around the skeg, transom and other regions where grid points need to be concentrated due to geometric complexity. Although these difficulties can be overcome, as demonstrated here, it becomes necessary to increase the overall number of grid points or sacrifice the grid resolution in the boundary layer. An initial grid of approximately 2.5 million points, which is split into 44 blocks for parallel processing, is used for the bare hull computations at model scale only. A finer grid of 5.9 million points, split into 84 blocks for parallel processing, is used when the bilge keels are added. This grid is used for both model and full-scale calculations with the points clustered more to the wall for the full scale as already discussed. This tighter clustering pulls more points closer to the wall, which leads to coarser grids away from the hull. Hence resolution of far field flow features can be compromised. The final grid of 7.2 million points includes the outboard

shaft. To include the shaft, cylindrical grids wrapping around the shafts are imbedded into the hull-conforming grid. Some idea of the complexity involved in this is shown in Fig. 5, which demonstrates how sections around the shaft need to be blocked out for grid generation. Here some of the grid surfaces that are near the hull upstream of the shaft leave the hull at the start of the shaft and move outward away from the hull with the shaft to maintain grid clustering around the shaft sufficient to capture flow physics. This clustering is displayed in Fig. 6, which compares the bare hull grid to the grid with the outboard shaft. Again, both grids have 129 points going out radially from the hull to the far field. Only a single grid is generated for the case with shaft. A second grid reclustered to the walls for full scale calculations is not generated. However, full scale calculations are performed on this grid and the results presented in later sections. Additionally, only the outboard shaft is included. This grid with the outboard shaft is split into 160 blocks for parallel processing.

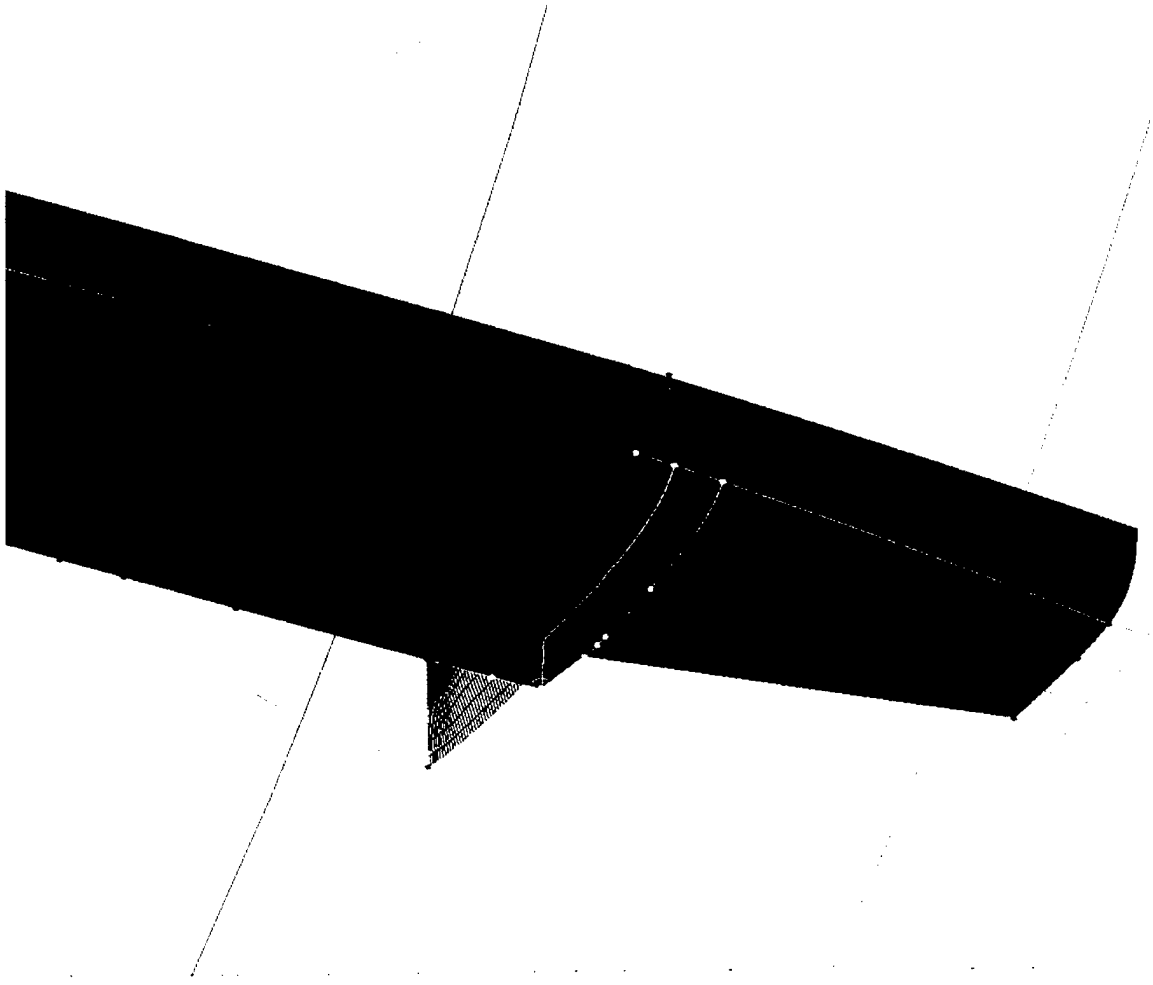

Fig. 5 Grid blocking scheme for the hull with shaft.

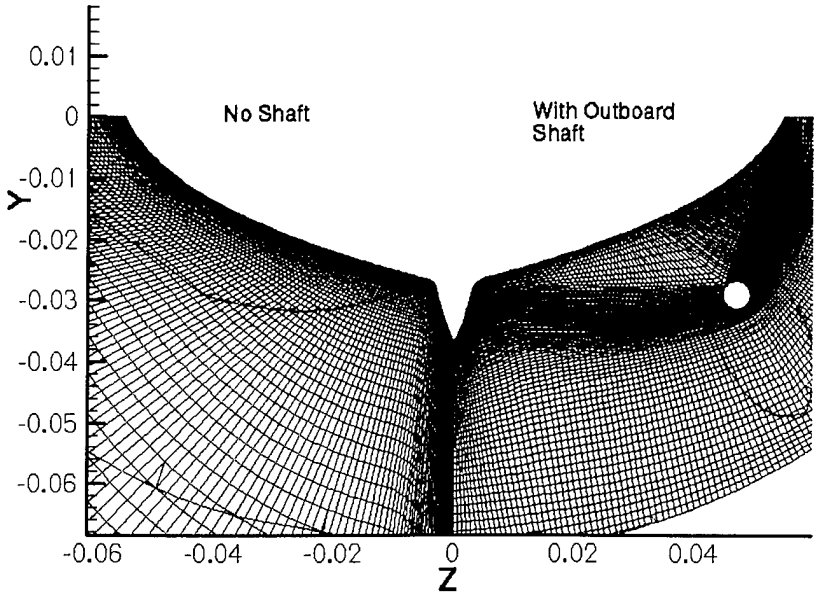

Fig. 6 Cross section of grid with and without outboard shaft.

FLOW SOLUTIONS

For this effort all calculations are for straight ahead flow with no angles of yaw. The hull is sunk and trimmed appropriately, based on experimentally obtained values, and run at model- and full-scale Reynolds numbers based on hull length of 35 x 10^6 and 48 x 10^8, respectively. Both cases are for a Froude number of 0.277 when using the linearized free surface boundary condition where the grid is generated up to the design waterline. The computed free surface elevations for the model scale prediction are shown in Fig. 7. This computed free surface height along the hull agrees well with experimentally observed data[14] (Fig. 8). Computed full-scale wave heights are very similar to those for model-scale. Individual hull effects are evaluated by performing a number of calculations. These include a coarse grid bare hull calculation without bilge keels and a fine grid calculation of the bare hull with bilge keels. Both of these bare hull calculations include the skeg and are performed at model and full-scale on the finer grid. The outboard propeller shaft is also included for a number of calculations. The inclusion of the outboard shaft had little impact on the computed free surface heights. With the outboard propeller shaft present propelled calculations are done using an actuator disk model with and without the shaft rotating. Again, these calculations are performed at both model and full scales.

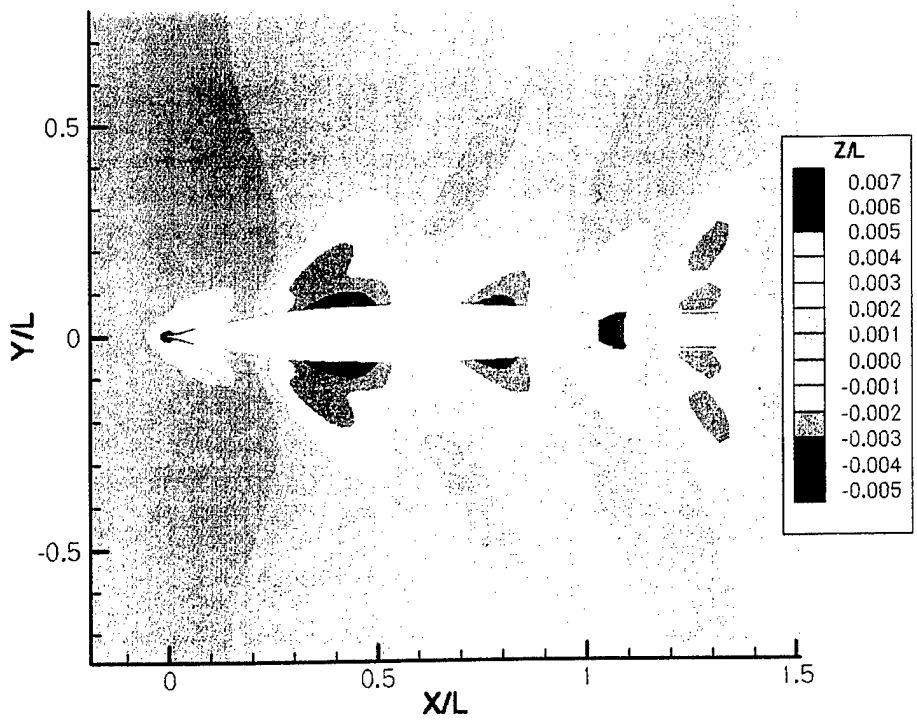

Fig. 7 Computed wave heights.

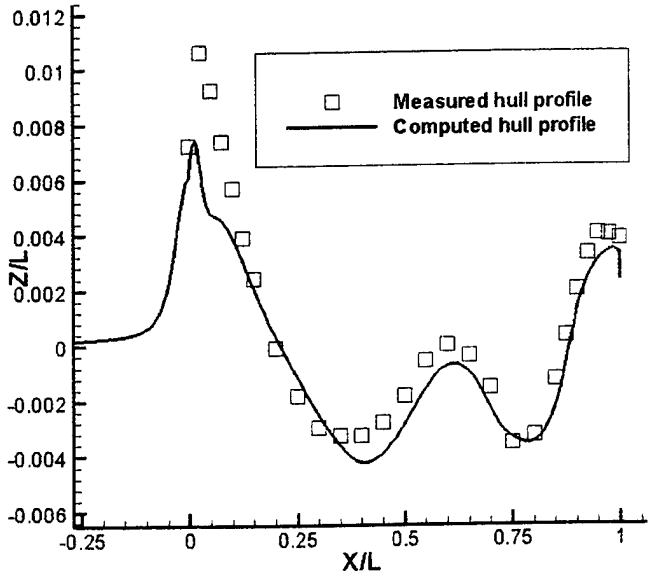

Fig. 8 Computed hull free surface height as compared with experimental data.

Bare Hull Model Scale Calculations

Model scale calculations, at Reynolds number of 35 x 10^6 based on length, are first done with the 2.5 million point grid without bilge keels. Results for the 5.9 million point grid, which includes bilge keels, are shown in Fig. 9. This figure shows surface streamlines and axial velocity contours at various locations along the length of the hull. It can be seen that the boundary layers are very thin even at model scale over most of the hull. Flow is generally downward over the forward part of the hull and then runs axially along the hull mid-section. An enlarged view of the bow area (Fig. 10) indicates that the downward flow creates a vortex over the bow dome that convects down the hull centerline. However, this vortex is rather weak and has negligible impact on the hull boundary layer midway down the length of the hull. The hull has rather sharp bilges and an expanded view of the midships region in Fig. 11 indicates a bilge vortex forming toward the stern of the hull. There appears to be some interaction between the bilge keel and the forming bilge vortex. However, the effects of the sharp bilge on the vortex formation seem to be more significant than the effects of the bilge keel. This bilge vortex travels downstream and is the dominant feature in the propeller plane area (Fig. 12). As shown, the wake retains much of the hull shape as it propagates downstream and takes on a very flat behavior at the stern on the underside except for the skeg wake. Due to the free surface interaction, there is a downward component of the flow at the stern, and then an upward flow toward the transom. The bilge/bilge keel vortex continues as a dominant feature into the wake.

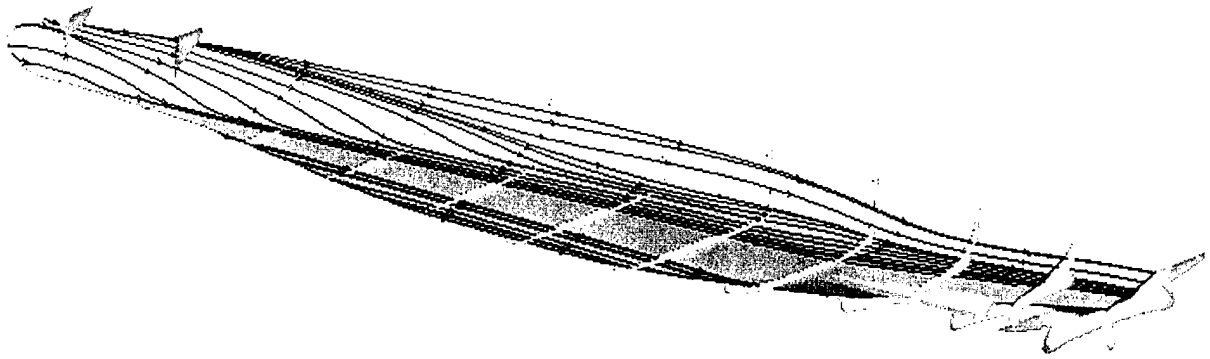

Fig. 9 Surface streamlines and axial velocity contours for the model scale calculation.

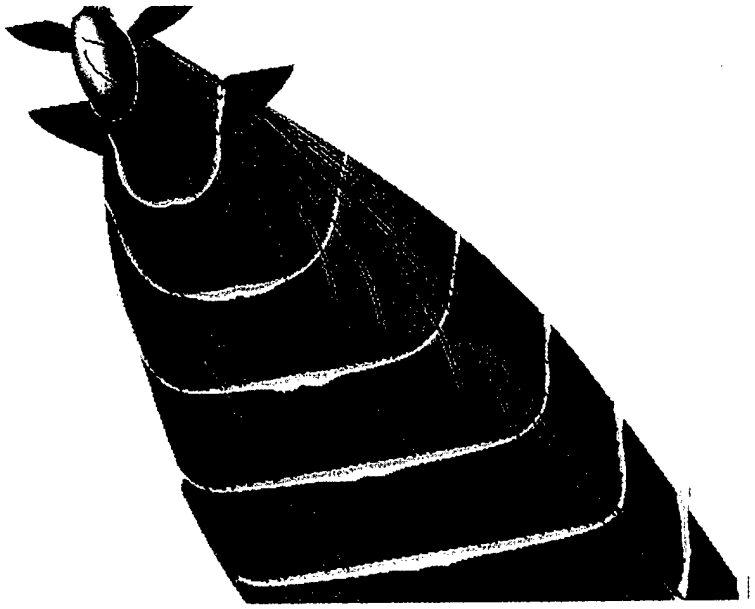

Fig. 10 Flow field in the bow region.

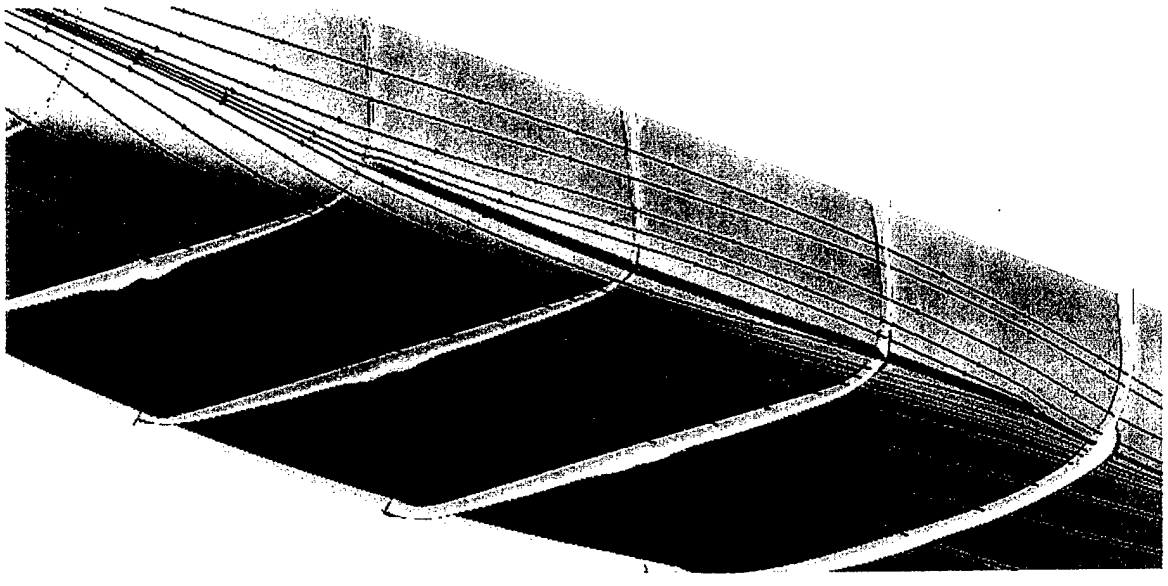

Fig. 11 Flow field in the midships region.

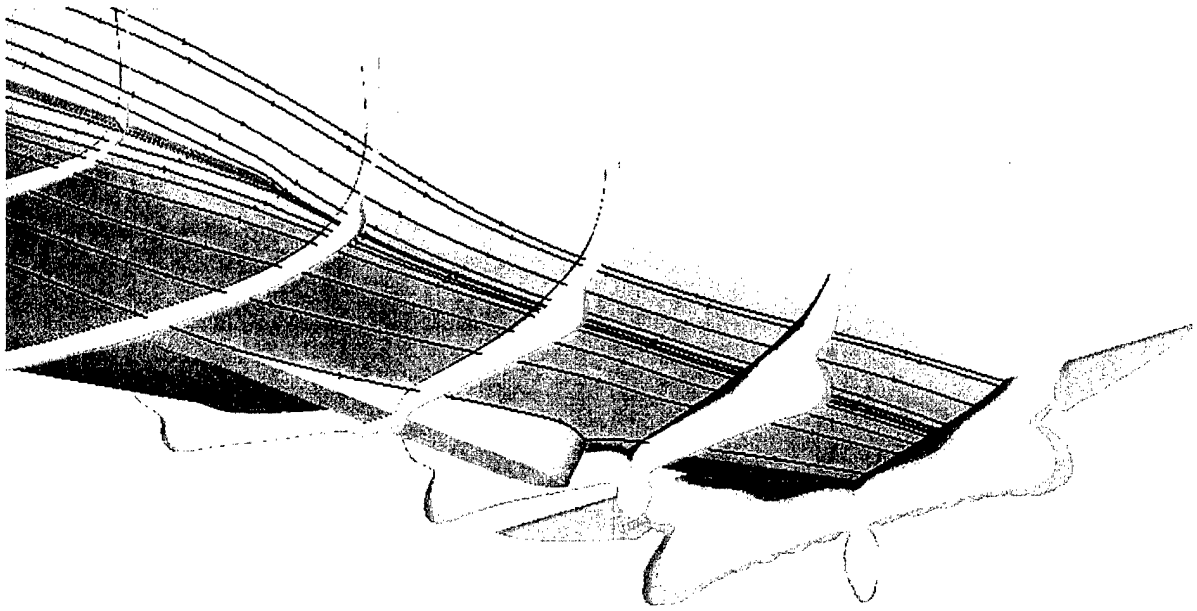

Fig. 12 Flow field in the stern region at model scale.

The bilge keel can be affecting the wake at the propeller disk. A cross section at X/L = 0.5 (Fig. 13) shows that there is still some secondary flow from the bow dome vortex which creates flow outward from the centerline towards the bilges. It can be seen in a cross section at X/L = 0.55 (Fig. 14) that the generally outward and upward flow around the bilge creates the downstream vortical flow and it appears the bilge keel significantly effects this. However, the bilge keel effect is apparently smaller than the effect due to the bilge itself. This is discerned from a comparison of the axial velocity contours at the inboard propeller plane for the calculation without bilge keels on the 2.5 million point grid, (Fig. 15), with those of the computation on the 5.9 million point grid with the bilge keels (Fig. 16). There are differences between the two, but the differences are quite likely due to the grid resolution differences as much as the bilge keel effect. The finer grid appears to predict a somewhat stronger bilge vortex as well as a more pronounced skeg effect, which is consistent with better grid resolution. One visible difference is a slight bulge in the velocity contours for the fine grid around Z = 0.05 which might be due to interaction with the free surface. Also shown in these two figures are measured axial velocity contours at the inboard propeller plane, which are overlaid on the computed contours. As can be seen the measured data is significantly different than that computed. The measured data has very obvious shaft and strut effects while the computed contours are relatively flat and conform to the hull shape as already discussed. Shown in Fig. 17 are axial velocity contours at the outboard propeller plane with the propeller disk location outlined. As seen the bilge vortex and hull wake significantly impact the flow into the propeller disk. The comparison with measured data at the outboard plane is better (Fig. 18) than at the inboard plane. The predicted boundary layer is somewhat thinner than measured, but has more of the characteristics of the measured data than at the inboard plane. However, there are still significant differences, some of which can be attributed to the shaft, as shown later.

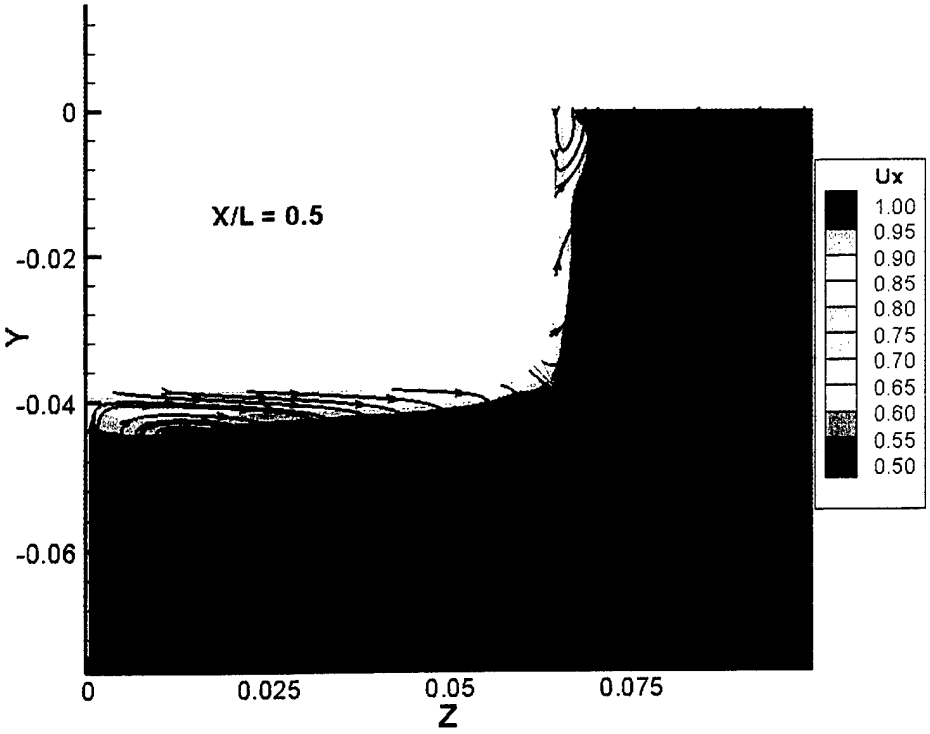

Fig. 13 Axial velocity contours and secondary flow streamlines at X/L = 0.5.

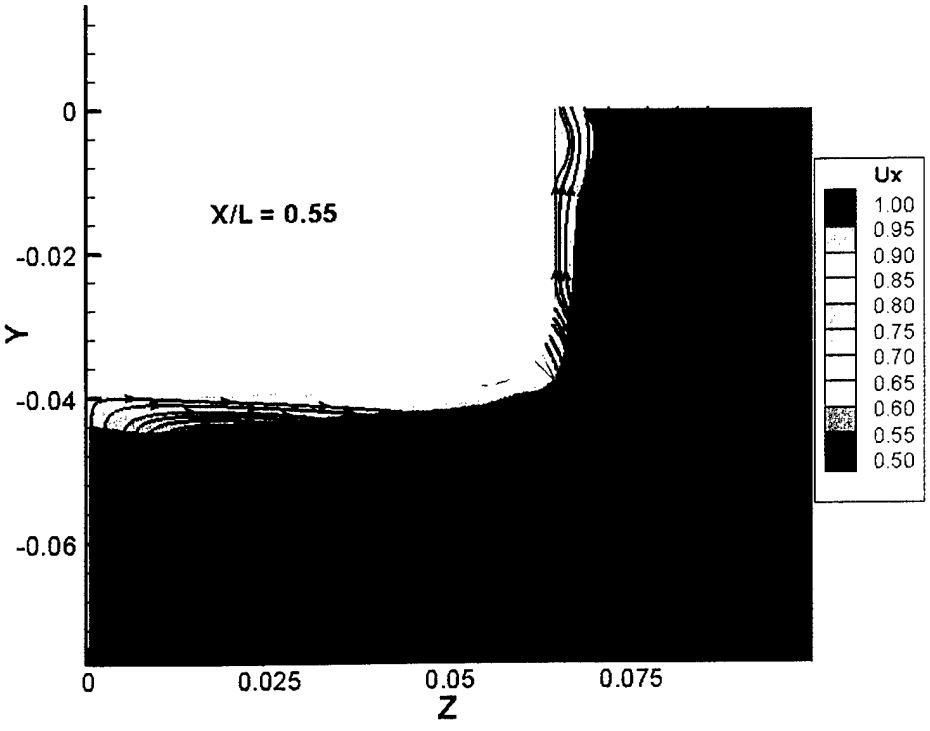

Fig. 14 Axial velocity contours and secondary flow streamlines at X/L = 0.55.

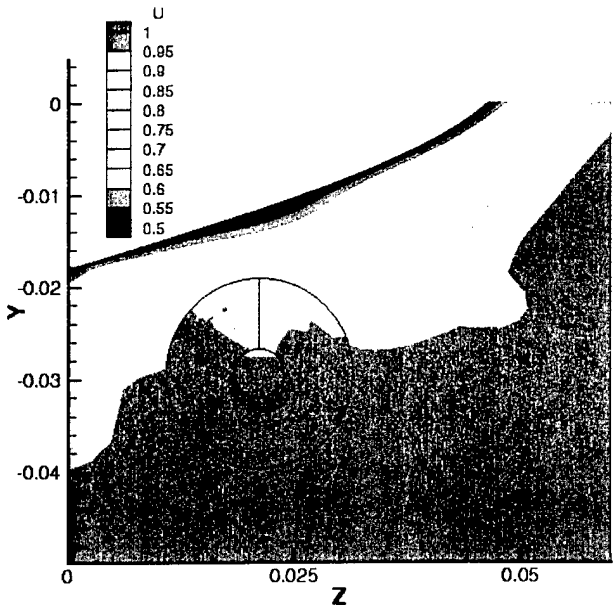

Fig. 15 Axial velocity contours at the inboard propeller plane computed without bilge keels compared with measured[14] contours in the propeller disk.

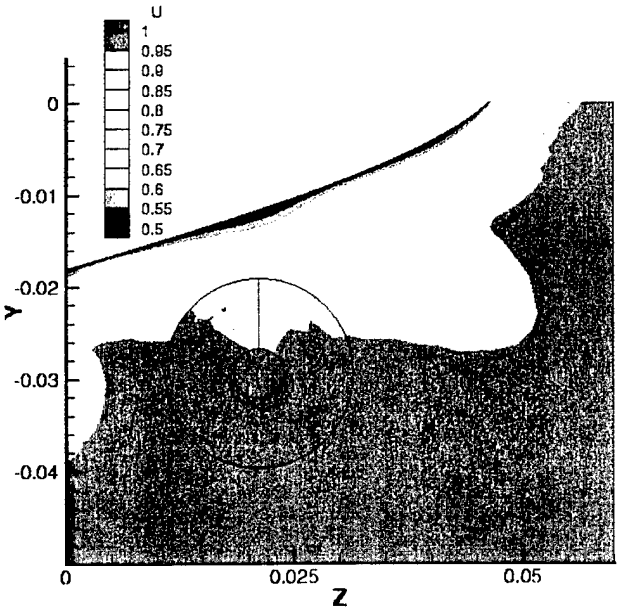

Fig. 16 Axial velocity contours at the inboard propeller plane computed with bilge keels compared with measured[14] contours in the propeller disk.

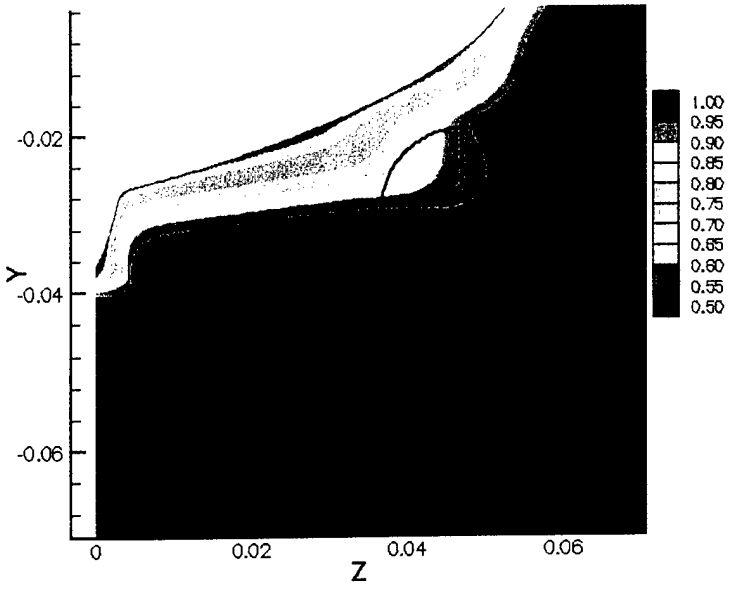

Fig. 17 Axial velocity contours at the outboard propeller plane computed with bilge keels.

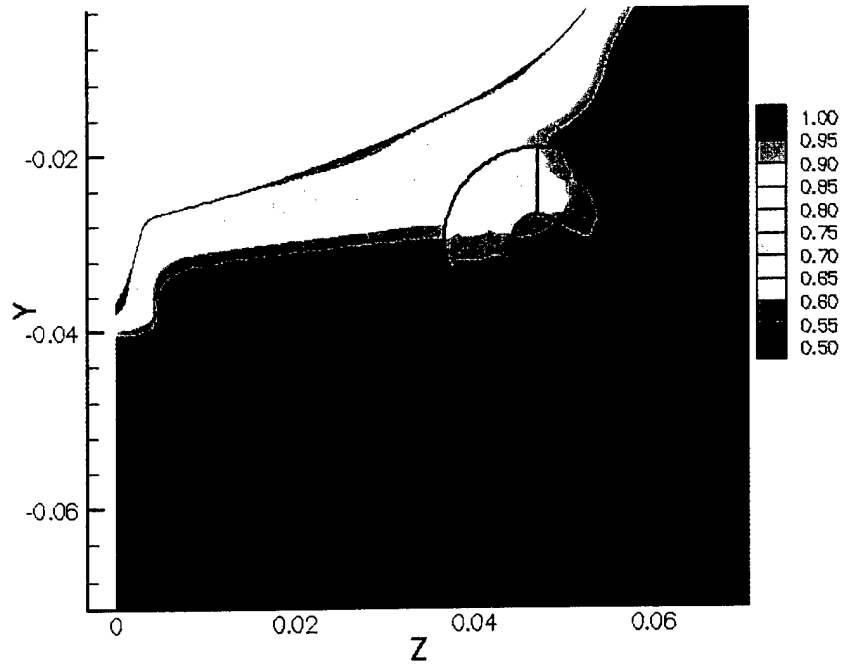

Fig. 18 Computed axial velocity contours at the outboard propeller plane compared with measured[14] contours in the propeller disk.

Bare Hull Full Scale Calculations

Full-scale calculations, at Reynolds number 48 x 10^8 based on length, are done with the 5.9 million point grid, which includes bilge keels. This grid has the same structure as the model scale grid, but has been more tightly clustered to the hull as already discussed. At full-scale the boundary layers are relatively thinner than at model scale so the bow vortex is less noticeable than that for the model scale computation. A view at the stern, shown in Fig. 19, indicates the formation of a bilge/bilge keel vortex. However, this is the only feature that stands out and the boundary layer wake of the hull is almost nonexistent. This feature appears to be a bilge vortex at the stern and not due to the presence of the bilge keel. There is some interaction between the bilge keel and bilge vortex forming, but the effect of the sharp bilge appears to be more significant than effects due to the bilge keel. There is a skeg wake, but it does not interfere with the propeller disks. The surface streamlines look very similar to those at model scale, but the flow at the propeller planes is significantly different than that seen at model scale. At the inboard plane the propeller disk basically experiences inviscid flow (Fig. 20) at the local angle of attack due to the hull shape. At the outboard propeller plane there is a slight perturbation to the inviscid flow, due to the bilge vortex, but this is negligible (Fig. 21). From these calculations it is obvious that there is a tremendous difference between model and full-scale predictions. The computations and turbulence models should be able to predict the correct trends with Reynolds number so some of this is the reality of the scale effects. However, as discussed by Gorski[3] one must consider the fact that such full-scale calculations do not account for roughness effects which can be significant on a real ship. Consequently, the real propeller inflow and hull wake is probably somewhere between these calculations. As seen from the comparisons with the experimental data these bare hull computations at model scale do not represent the measured data to a high degree of fidelity. This discrepancy is primarily due to shaft and strut effects, which can be significant, as shown in the next section.

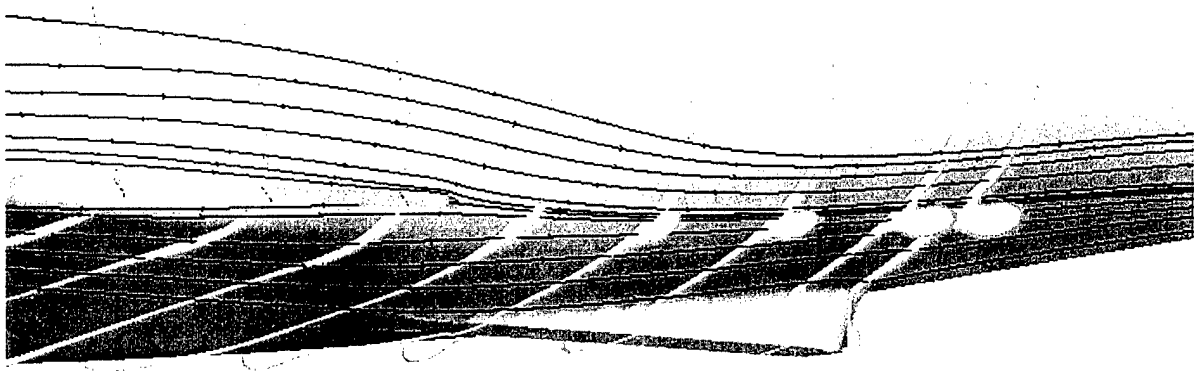

Fig. 19 Axial velocity contours and surface streamlines for the full-scale calculation.

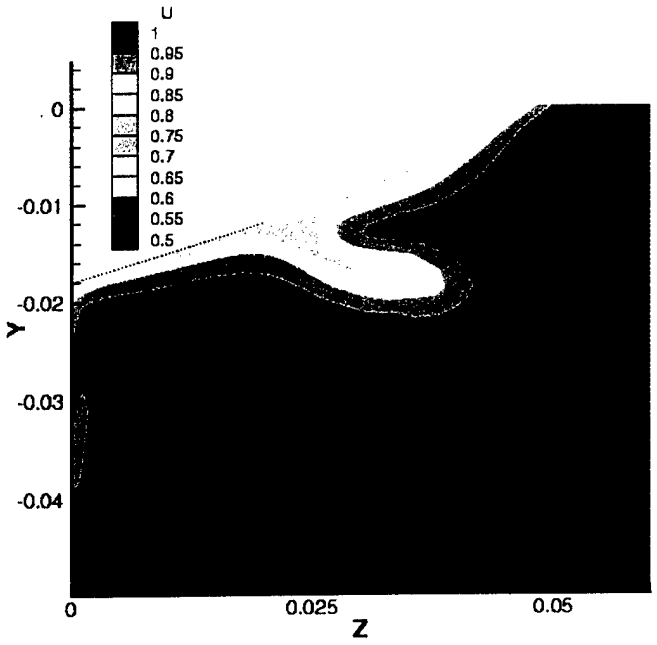

Fig. 20 Axial velocity contours at the inboard propeller plane.

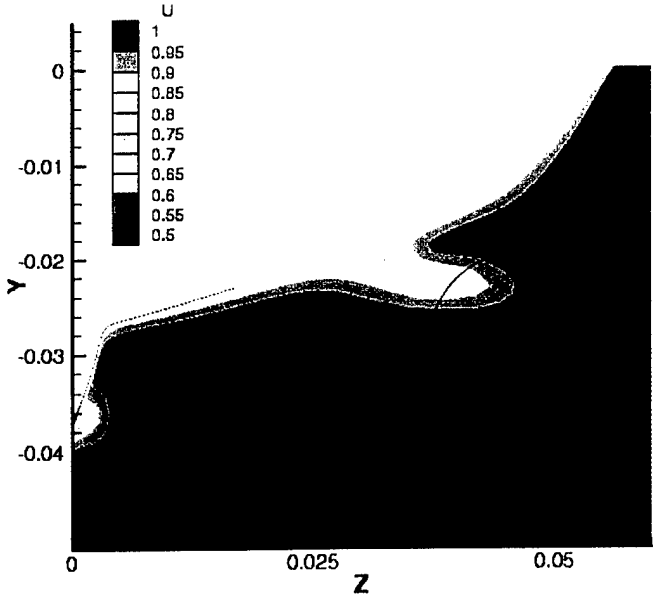

Fig. 21 Axial velocity contours at the outboard propeller plane.

Outboard Shaft Effects

Calculations are performed at both model and full-scale including the outboard shaft. The inboard shaft is not modeled nor the outboard shaft supporting struts. The grid consists of 7.2 million grid points for half the geometry. Computed axial velocity contours near the stern of this hull are shown in Fig. 22. It is seen that the bilge/bilge keel vortex flow that is the dominant feature at the stern for the bare hull configuration flows directly into the outboard shaft. The shaft changes this flow significantly creating an additional wake deficit in the outboard propeller disk. A comparison of the bare hull axial velocity contours and those of the current configuration are shown in Fig. 23. There is a velocity deficit between the hull and shaft, which is not present in the bare hull calculation. This wake deficit appears to be a shaft wake. One must remember that the flow at this location has a strong upward component due to the hull draft rapidly decreasing toward the stern. The flow follows the hull form and its vertical component creates a wake due to the shaft, between the shaft and the hull, as seen from the secondary flow vectors of Fig. 24. This added velocity deficit leads to a much better comparison of these results, with the experimental data, than such a comparison of the bare hull results. This is demonstrated in Fig. 25, which shows slices of the computed axial velocity for the bare hull and shafted hull on the same cross section as the measured data at the outboard propeller plane. The bare hull flow has none of the sharp wake-like velocity deficit. The computation with the shaft agrees well with the measured data, which also has the wake-like deficit. The measured data has a somewhat wider wake, which is probably due to the struts. However, the similarity of the computed flow without struts and the measured data with struts indicates the strut effect is secondary to the shaft effect.

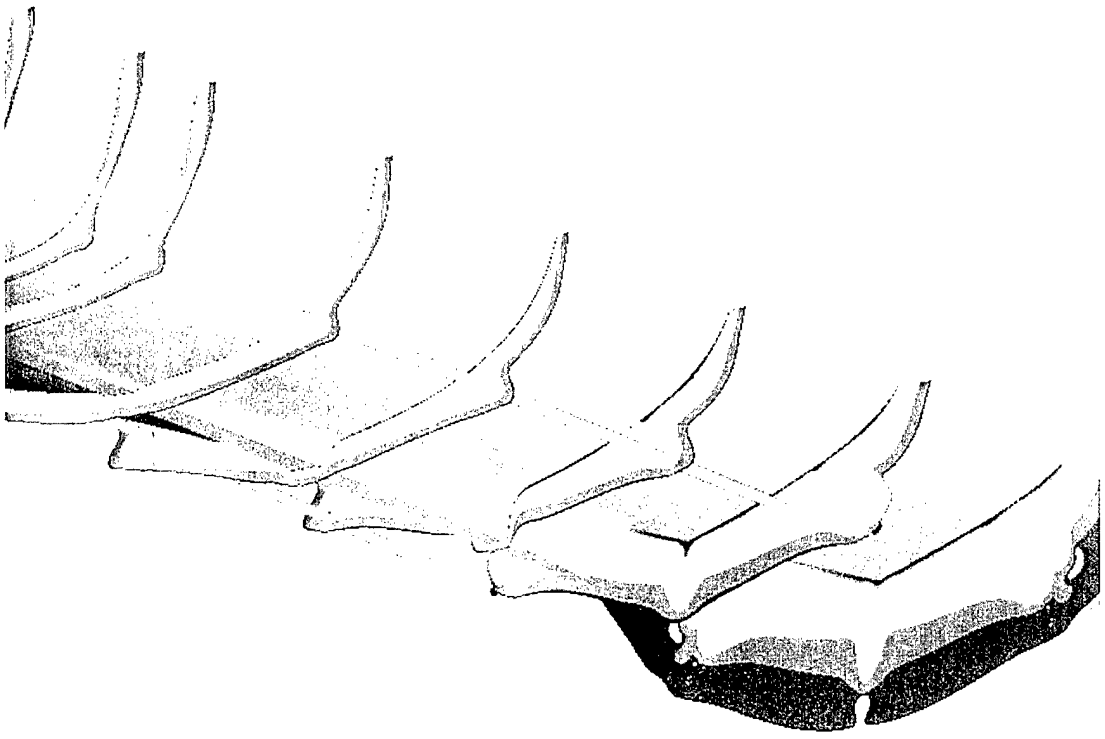

Fig. 22 Computed axial velocity contours with the outboard shaft at model scale.

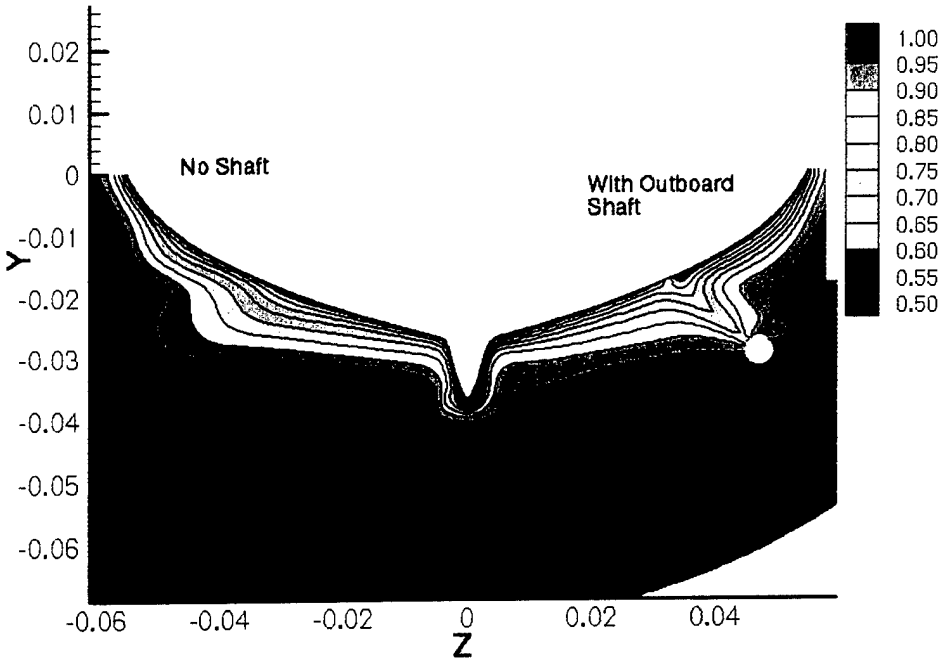

Fig. 23 Comparison of axial velocity at outboard propeller plane with/without shaft.

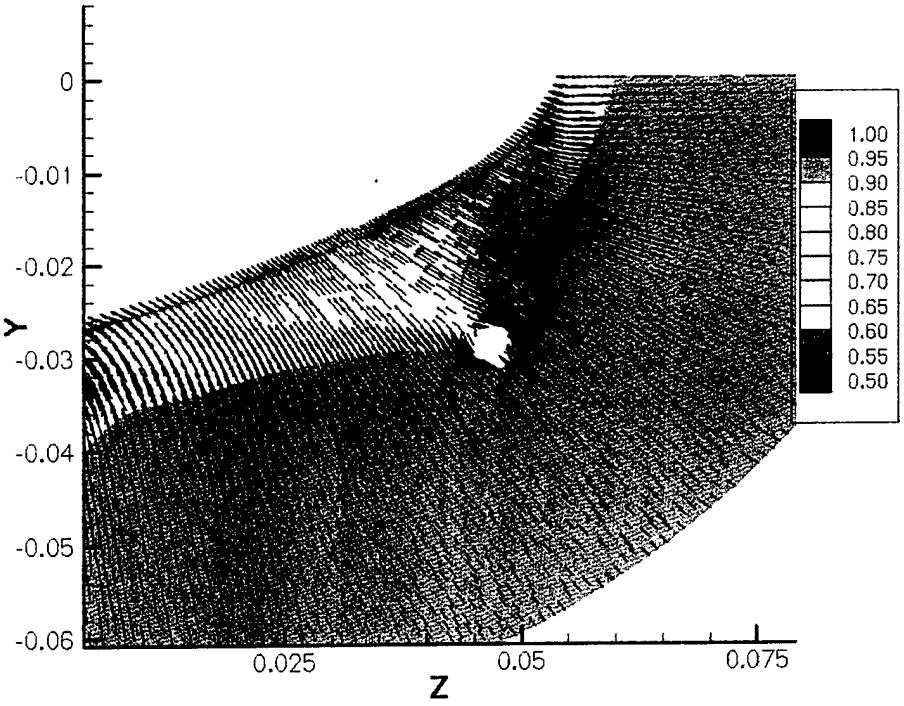

Fig. 24 Secondary velocity vectors at the outboard propeller plane.

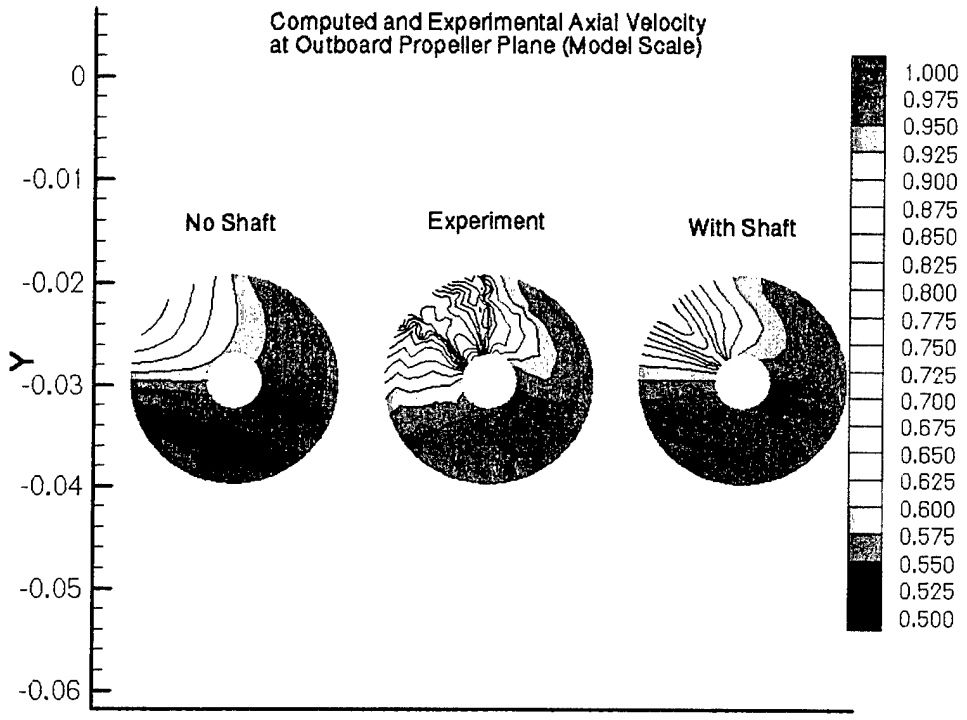

Fig. 25 Computed and measured[14] axial velocity at the outboard propeller plane.

Also seen in Fig. 22 is a noticeable effect on the flow downstream of the outboard propeller shaft, due to the interaction of the bilge vortex and shaft. As a result flow at the inboard propeller plane is influenced by the outboard shaft (Fig. 26). There is also an apparently thicker boundary layer than obtained with the bare hull computation and there appears to be some interaction between the outboard shaft and the skeg. This downstream flow due to the outboard shaft does impact the inboard propeller plane disk as seen in Fig. 27. However, comparison of the bare hull computation and shafted computation with measured data at the inboard propeller disk still shows that the dominant feature in the measured data is the wake of the inboard shaft and strut. It is interesting to note (Fig. 26) that at the outboard propeller plane also the computed flow with the shaft shows a thicker boundary layer on the hull underside than the unrealistically thin layer for the bare hull computation.

The full-scale calculations with shaft are done on the same grid as used for the model scale calculations so the clustering near the wall is less than satisfactory. This calculation again showed largely inviscid flow at the propeller with some slight effect due to the shaft. These features will be discussed further in conjunction with the propelled calculations.

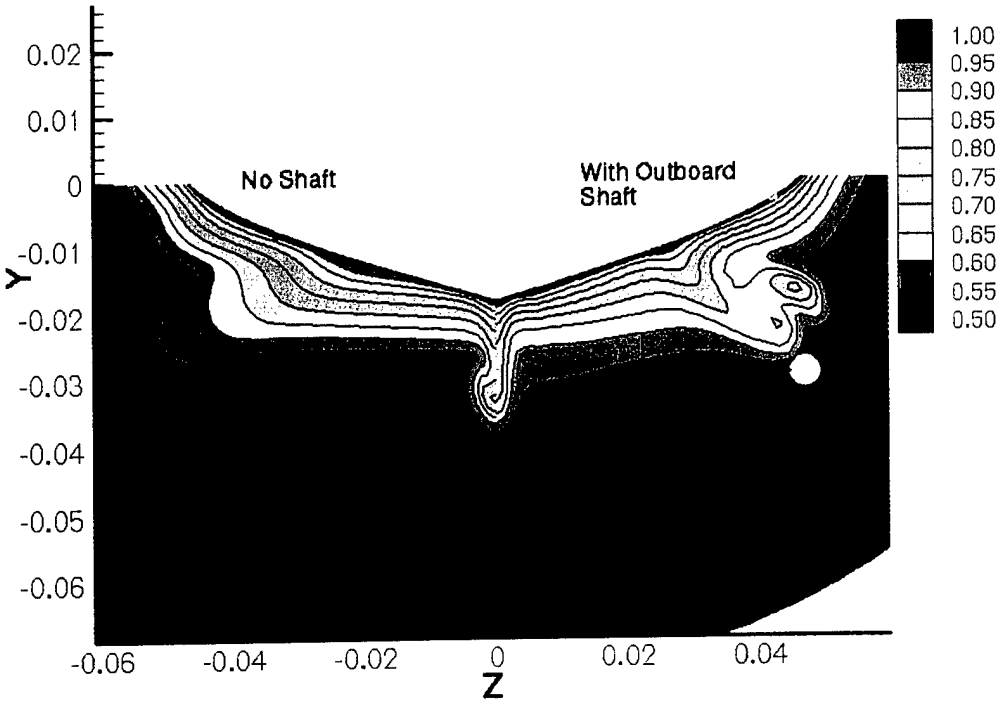

Fig. 26 Computed axial velocity contours at the inboard propeller plane.

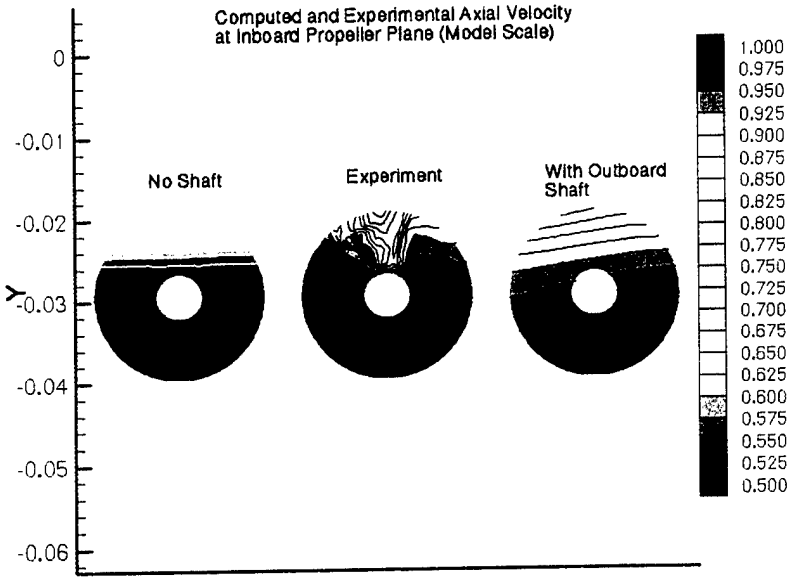

Fig. 27 Comparison of axial velocity at the inboard propeller plane.

Propeller Modeling

Calculations are performed at both model and full scale with the outboard propeller modeled as an actuator disk. These calculations are done with the outboard shaft present, but not rotating. With the actuator disk model a single grid plane is chosen at the propeller plane and a constant Kt and Kq imposed over the disk in this plane. With this approach the total Kt and Kq imposed over the disk is at the correct level, but a constant value is imposed so there is no accounting for radial distributions of force. Additionally, different levels of thrust and torque produced in the inner part of the disk interacting with the hull/shaft wake are not modeled differently than that exposed to the free stream flow. Shown in Fig. 28 are the computed axial velocity contours at the outboard propeller plane at model scale. The propeller modeling accelerates the flow to above free stream levels over most of the disk area. However, the wake of the hull and outboard shaft are still present and provide a velocity deficit over approximately 90° of the disk area. The secondary flow is also changed due to the rotation of the propeller, as show in Fig. 29, but the shaft wake deficit stays in much the same position as in the unpropelled case. The full-scale calculation, Fig. 30, shows a largely inviscid flow as expected. The axial velocity has increased to similar levels as in the model scale calculation. However, the velocity deficit due to the hull/shaft wake which exists at model scale is largely nonexistent at full-scale.

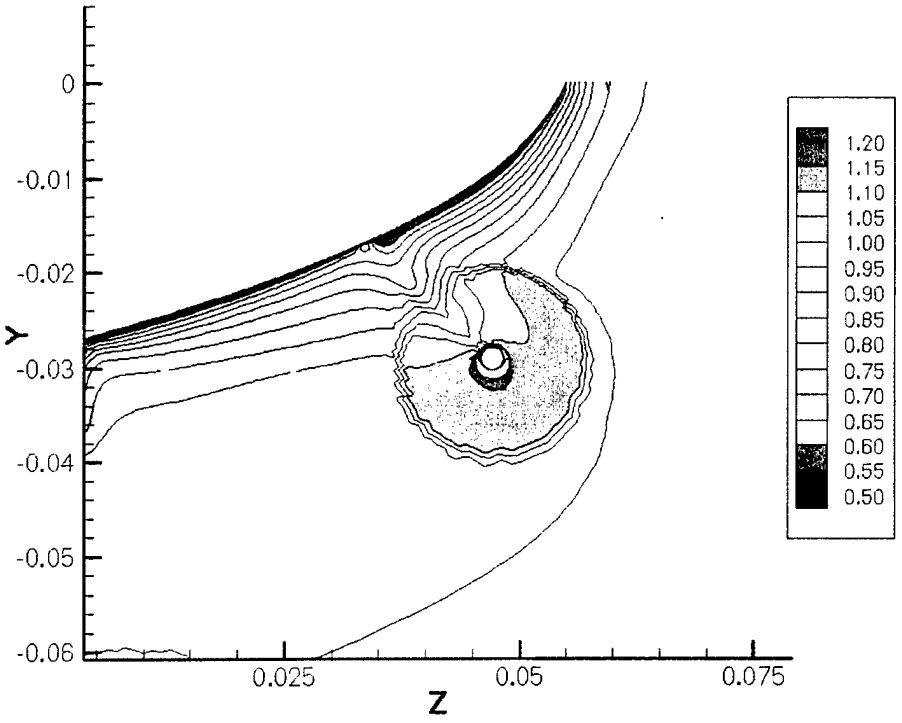

Fig. 28 Model scale axial velocity with the outboard propeller modeled.

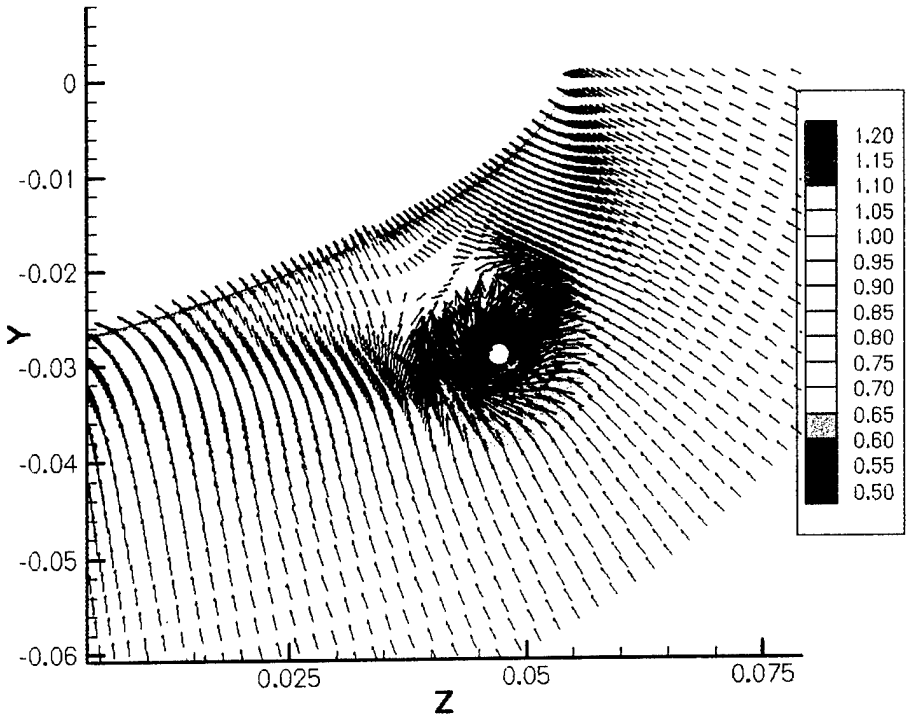

Fig. 29 Secondary velocity vectors with the outboard propeller modeled.

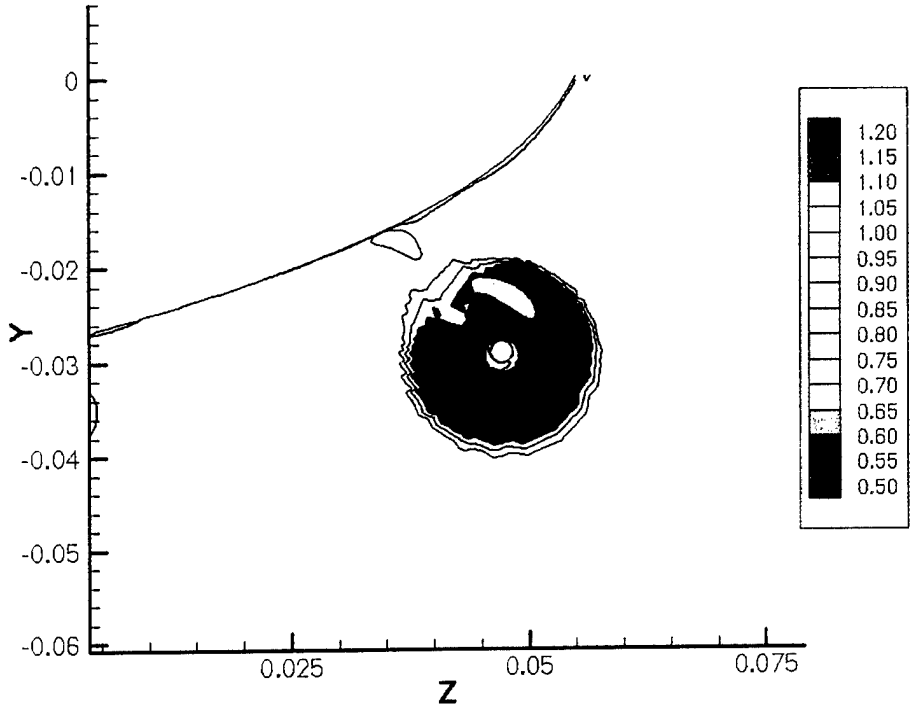

Fig. 30 Full scale axial velocity contours with the outboard propeller modeled.

Shaft Rotation Effects

The previous propelled calculations are performed without shaft rotation. Additional calculations are performed using the same actuator disk model, but with the shaft rotating. The shaft rotation has an effect on the flow. Axial velocity contours for the model scale calculation, near the shaft, are shown in Fig. 31. This calculation also includes the propeller modeled with an actuator disk near the end of the shaft. As seen, the wake of the shaft between the shaft and hull, is pulled around by the shaft to create a curved wake due to the shaft rotation. At the propeller plane the model scale prediction shown in Fig. 32 has a similar overall wake deficit in the top of the propeller disk as for the fixed shaft. However, the low velocity middle of the wake has become thinner with lower velocity reaching to the shaft. This appears to be a result of the shaft rotation, and the subsequent no-slip boundary condition on the shaft, pulling more low momentum flow from the area between the shaft and the hull down toward the shaft. Here it is also apparent that this shaft wake has rotated around with the shaft somewhat from its previous position when the shaft is fixed. This wake rotation is also apparent with the full-scale calculation, Fig. 33. Here a wake defect appears due to the shaft, which is not apparent in the full-scale case without shaft rotation. This velocity deficit is very thin, but does change the flow from the cleaner free-stream type flow seen without the shaft rotation at full scale.

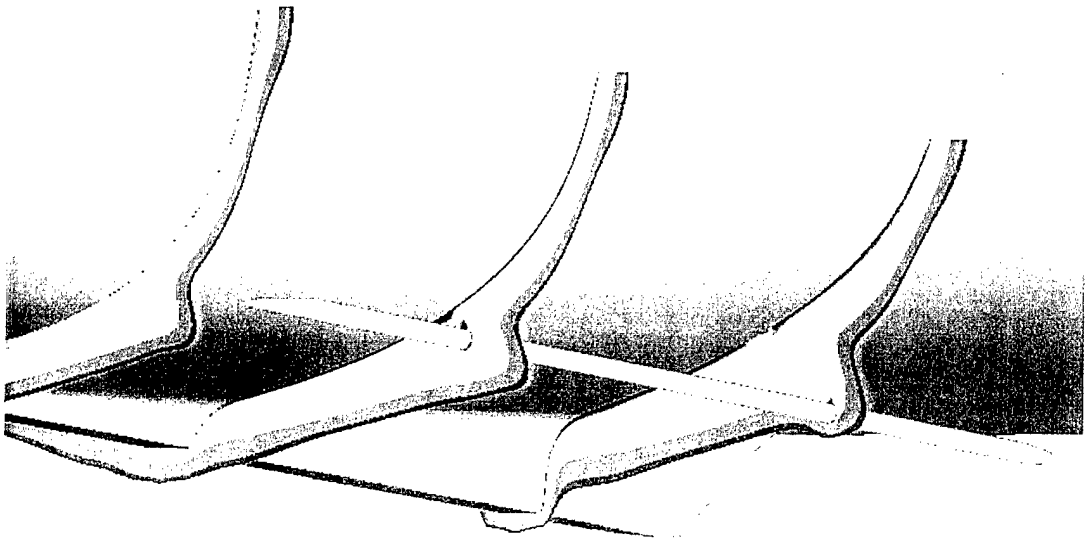

Fig. 31 Axial velocity contours with the shaft rotating.

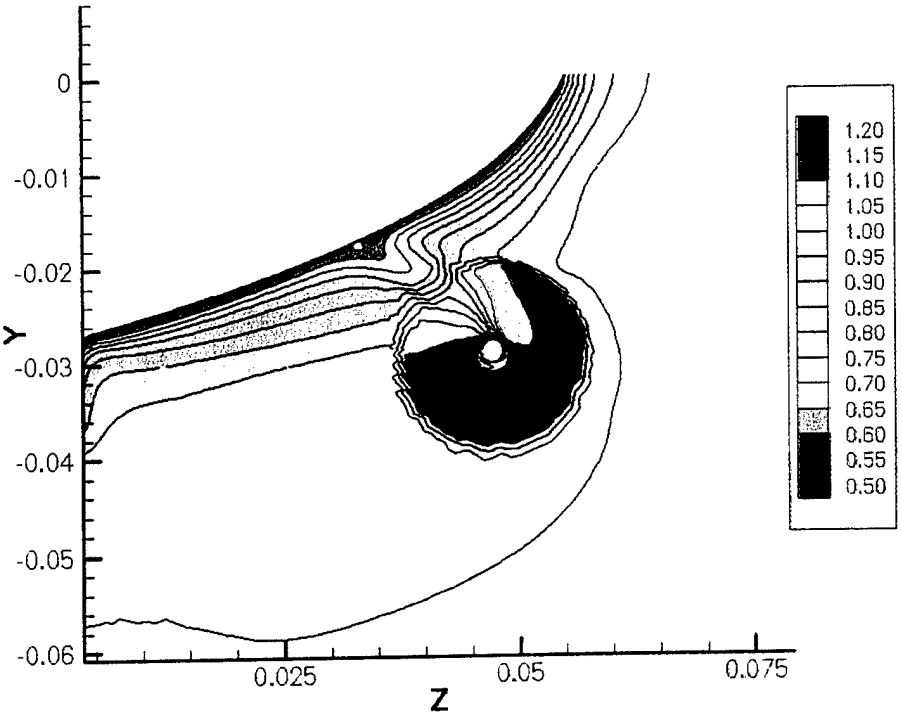

Fig. 32 Model scale calculation with shaft rotation.

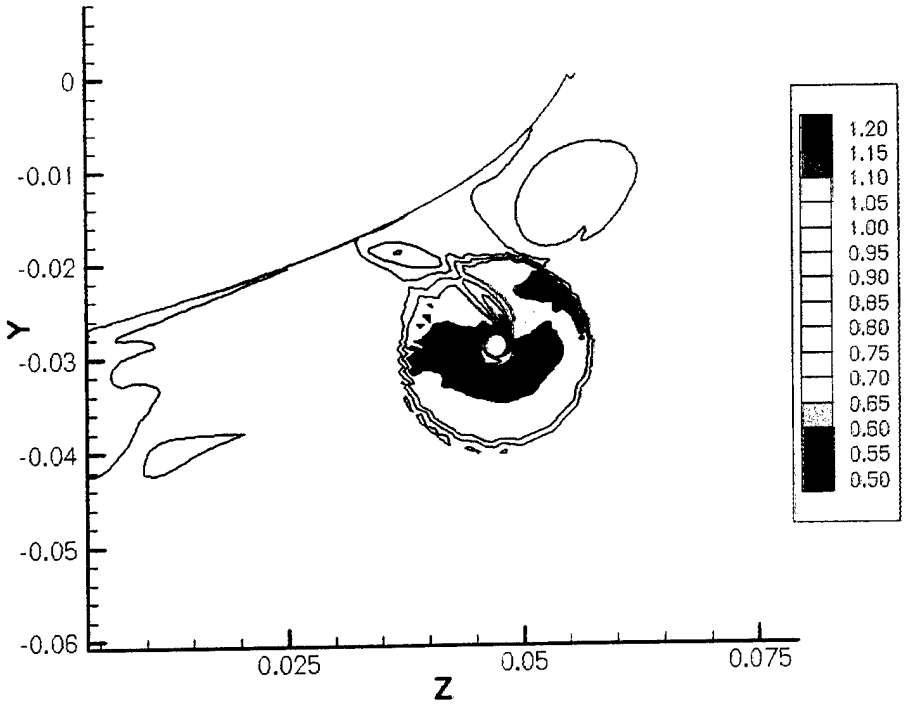

Fig. 33 Full-scale calculation with shaft rotation.

CONCLUSIONS

RANS calculations are performed for a carrier hull configuration at model and full scale Reynolds numbers. The hull includes the bow dome, skeg, bilge keels, and outboard shaft. Comparisons are made with and without bilge keels as well as with and without the outboard shaft. Significant differences are observed in the calculations due to changes in Reynolds number from model to full scale. The model scale calculations demonstrate a significant hull wake entering both inboard and outboard propeller planes. At the outboard propeller plane the hull wake entering the disk is complicated by a bilge/bilge keel vortex formed upstream. The full scale calculations show nearly inviscid flow entering the propeller disks with minimal hull boundary layer and wake. From this one could conclude that measured model scale inflow to the propeller planes has a larger wake deficit than seen at full scale. However, these full scale calculations do not account for surface roughness which can lead to thicker full scale boundary layers than predicted.

The shafts also impact the propeller inflow and appear to be more significant than the hull boundary layer and wake effects. The model-scale calculations without the inboard shaft show a rather benign boundary layer flow at the inboard propeller plane, whereas the experimental data demonstrates a significant shaft wake. This relative importance of the shaft is confirmed at the outboard propeller plane where the model scale computation with the shaft agrees reasonably well with measured data, both of which demonstrate a wake due to the shaft. From these comparisons it appears the added effect of the shaft struts may be secondary as long as the struts are aligned with the flow. The shaft rotation enhances this wake effect. Again, though, the full scale calculations are significantly different than the model scale and demonstrate nearly inviscid flow entering the propeller disks even with the shaft present. However, shaft rotation does show up in the full scale calculations creating a wake between the hull and shaft and providing a wake deficit not seen without the shaft rotation.

One thing that needs to be considered when using RANS codes for such complicated geometries is the ability to quickly grid the various important details. The current geometry with its shafts and struts could not be gridded properly in the time frame allocated using structured grids. Consequently, there was an emphasis on bare hull calculations. Even so, the RANS calculations seem to provide some very believable and useful information concerning flow physics and scale effects. However, it is apparent that the local flow due to the shafts and struts is important to the propeller inflow and needs to be included in calculations relevant to the real hull form. To achieve this, the ability to generate good grids for complicated geometries must be more automated. Unstructured grid technology provides the possibility of achieving this and can be used for such complications in the future as confidence is gained in unstructured codes for accurately predicting viscous effects.

ACKNOWLEDGEMENTS

This work was supported in part by a grant of computer time at the Arctic Region Supercomputing Center provided by the DOD High Performance Computing Modernization Office under the Project CFD for Naval Vehicles. Software licenses for GRIDGEN were provided by the U.S. Navy Hydrodynamic/Hydroacoustic Technology Center.

THIS PAGE INTENTIONALLY LEFT BLANK

REFERENCES

1 Gorski, J. J., "Marine Vortices and Their Computation," Presented at the NATO RTO Applied Vehicle Technology Panel Symposium on Advanced Flow Management, Loen, Norway, May, 2001.

2 ITTC, 1996, "Report of the Resistance and Flow Committee," *Proc. 21st ITTC*, Trondheim, Norway.

3 Gorski, J. J., "Present State of Numerical Ship Hydrodynamics and Validation Experiments," Proceedings of OMAE'01 20th Int. Conf. Offshore Mechanics and Arctic Engineering, Rio de Janeiro, Brazil, OMAE01/OFT-1350, June, 2001.

4 Roache, P. J.,1998, *Verification and Validation in Computational Science and Engineering*, Hermosa Publishers, Albuquerque, New Mexico.

5 AIAA, 1998, *Guide for the Verification and Validation of Computational Fluid Dynamics Simulations*, G-077-1998.

6 Taylor, L. K. and D. L. Whitfield, "Unsteady Three-Dimensional Incompressible Euler and Navier-Stokes Solver for Stationary and Dynamic Grids," AIAA Paper No. 91-1650, (June 1991).

7 Taylor, L. K., A. Arabshahi, and D. L. Whitfield, "Unsteady Three-Dimensional Incompressible Navier-Stokes Computations for a Prolate Spheroid Undergoing Time-Dependent Maneuvers," AIAA Paper No. 95-0313, (Jan. 1995).

8 Chorin, A. J., "A Numerical Method for Solving Incompressible Viscous Flow Problems," *Journal of Computational Physics*, Vol. 2, pp. 12-26, (1967).

9 Van Leer, B., J. L. Thomas, P. L. Roe, and R. W. Newsome, "A Comparison of Numerical Flux Formulas for the Euler and Navier-Stokes Equations," AIAA Paper No. 87-1104-CP, (June 1987).

10 Whitfield, D. L. and L. K. Taylor, "Discretized Newton-Relaxation Solution of High Resolution Flux-Difference Split Schemes," AIAA Paper No. 91-1539, (June 1991).

11 Sheng, C., L. Taylor, and D. Whitfield, "Multiblock Multigrid Solution of Three-Dimensional Incompressible Turbulent Flows About Appended Submarine Configurations," AIAA Paper No. 95-0203, (Jan. 1995).

12 Taylor, L., K., et al., "Large-Scale Simulations for Maneuvering Submarines and Propulsors," AIAA Paper No. 98-2930, (1998).

13 Patel, V. C., 1998, "Perspective: Flow at High Reynolds Number and Over Rough Surfaces – Achilles Heel of CFD," *J. Fluids Eng.*, Vol. 120, pp. 434 – 444.

14 Experimental data provided courtesy of Code 5200, Naval Surface Warfare Center, Carderock Division, West Bethesda, MD.

THIS PAGE INTENTIONALLY LEFT BLANK

INITIAL DISTRIBUTION

Copies		Code	Name
1	NAVSEA	SEA05H	Crockett
1	NSWCCS		Hyman
2	ONR	333	Kim, Purtell
1	Electric Boat		Knight
1	Newport News		Burton
1	MSU		Whitfield
1	Univ. of Iowa		Stern
1	DTIC		

Division Distribution

1	342	TIC
1	5000	
1	5050	Reed
1	5010	Administrative Office
1	5060	Walden
2	5200	Karafiath, Ratcliffe
13	5400	Coleman, Ebert, Gorski (5), Jessup, Michael, Miller, Slomski, Szwerc, Telste